Available online at www.sciencedirect.com

ScienceDirect

IFAC PapersOnline CONFERENCE PAPER ARCHIVE

IFAC PapersOnLine 55-7 (2022) 869–874

Data-driven Models for Advanced Control of Acid Gas Treatment in Waste-to-energy Plants

Riccardo Bacci di Capaci [*,***] **Gabriele Pannocchia** [*]
Alessandro Dal Pozzo [**] **Giacomo Antonioni** [**] **Valerio Cozzani** [**]

[*] *Department of Civil and Industrial Engineering, University of Pisa, Italy*
[**] *Department of Civil, Chemical, Environmental and Material Engineering, University of Bologna, Italy*
[***] *Corresponding author: riccardo.bacci@unipi.it*

Abstract: This paper presents a study of identification and validation of data-driven models for the description of the acid gas treatment process, a key step of flue gas cleaning in waste-to-energy plants. The acid gas removal line of an Italian plant, based on the injection of hydrated lime, $Ca(OH)_2$, for the abatement of hydrogen chloride, HCl, is investigated. The final goal is to minimize the feed rate of reactant needed to achieve the required HCl removal performance, also reducing as a consequence the production of solid process residues. Process data are collected during dedicated plant tests carried out by imposing Generalized Binary Noise (GBN) sequences to the flow rate of $Ca(OH)_2$. Various input-output and state-space models are identified with success, and related model orders are optimized. The models are then validated on different datasets of routine plant operation. The proposed modeling approach appears reliable and promising for control purposes, once implemented into advanced model-based control structures.

Keywords: Process modeling; process control; waste incineration; acid gas removal

1. INTRODUCTION

Waste-to-energy (WtE) facilities are characterized by an extreme variability in flue gas composition, mostly given by the fluctuating content of acid gases such as HCl, SO_2, HF. Methods based on the injection of dry sorbents are nowadays considered among the best available techniques for acid gas removal (Dal Pozzo et al., 2018a). However, it is worth noting that industrial control algorithms are typically oriented to ensure high safety margins in compliance with strict emission standards rather than properly tracking a set-point of outlet pollutant concentration (Dal Pozzo et al., 2021). As a consequence, reactants are fed in large excess with respect to the stoichiometric demand in order to confidently neutralize acid pollutants and avoid possible overshoot in emissions at stack.

In the face of increasingly stringent emission standards, excess reactant feed is indeed becoming a major economic burden, as well as a source of indirect environmental impacts, in terms of excess production of solid process residues (Biganzoli et al., 2015; Dal Pozzo et al., 2017). Therefore, a question naturally arises: are there any margins for optimizing the reactant feed without affecting the pollutant removal performance? The answer is definitely affirmative, and advance control systems seem the natural solution for such type of industrial processes.

Dry systems for the removal of acid gases are typically composed of a reactor followed by a filtration unit for the separation of solid process residues (Dal Pozzo et al., 2016). Several WtE plants adopt a two-stage architecture, where the first stage usually employs hydrated lime as reactant, and the second one injects sodium bicarbonate. In order to maintain the required overall acid gas abatement efficiency, the first removal stage may become particularly critical, because the input content of hydrogen chloride (HCl) can be very fluctuating over time, depending on the composition of the solid waste entering the plant. The objective of an optimal operation of the first removal stage is twofold:

- reduce the consumption of hydrated lime and therefore the production of solid residues;
- reduce the variability of the output HCl concentration, which represents an input disturbance for the second stage with bicarbonate.

In particular, the main objective addressed in this paper is to develop suitable dynamic models of the gas removal unit, by using routine industrial input-output data and systems identification methods (Ljung, 1999). This task represents the first step for the design of different types of advanced model-based controllers, as Internal Model (IMC) and Model Predictive (MPC) solutions, which are supposed to replace the traditional industrial control architectures typically implemented in DCS of WtE plants. The paper is thus briefly organized as follows: the system definition is given in Section 2; while the main aspects of the proposed methodology, based on systems identification and validation, are illustrated in Section 3. Finally, Section 4 includes conclusions for the work.

2. SYSTEM DEFINITION

The main features of the system under study are here described.

2.1 The case study

The considered WtE plant is located in Northern Italy and presents a typical two-stage dry acid gas removal unit, composed of a sequence of reaction and filtration (see Figure 1).

10.1016/j.ifacol.2022.07.554

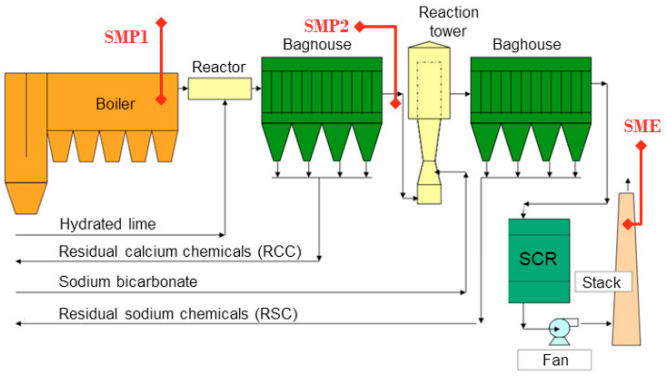

Fig. 1. Simplified flow diagram of the gas treatment line of the considered WtE plant.

The first stage adopts hydrated lime $Ca(OH)_2$ fed to a tubular reactor; the second step uses sodium bicarbonate $NaHCO_3$ injected into a reaction tower. Residual solid chemicals are separated from two bag filters by reverse pulse jet cleaning, i.e., calibrated blasts of compressed air. Three different measurement points for the flue gas composition are installed: the first sensor system is located at the boiler outlet (SMP1), the second one after the first baghouse (SMP2), the last one at the stack base (SME). Flue gases are composed of different acid components; in decreasing order of concentration, the sensors typically reveal HCl, NO, SO_2, HF, NO_2.

Among the various acid-base reactions happening within the first stage of removal, the ones involving hydrogen chloride are the most frequent. Modeling studies report the following three gas-solid reactions (Dal Pozzo et al., 2018b):

$$2HCl_{(g)} + Ca(OH)_{2(s)} \rightarrow CaCl_{2(s)} + 2H_2O_{(g)} \quad (1)$$

$$2HCl_{(g)} + Ca(OH)_{2(s)} \rightarrow CaCl_2 \cdot 2H_2O_{(s)} \quad (2)$$

$$2HCl_{(g)} + Ca(OH)_{2(s)} \rightarrow CaOHCl_{(s)} + H_2O_{(g)} \quad (3)$$

This reaction set generates significant solid residuals - anhydrous ($CaCl_2$) and dihydrate ($CaCl_2 \cdot 2H_2O$) calcium chloride, and calcium hydroxy chloride (CaOHCl) - which get deposited over the tissue of the bag filters forming an inert cake.

The variables measured online are sent to the control logic implemented in the DCS to regulate the $Ca(OH)_2$ feed rate. Flow rates and pollutant concentrations are not used as raw data, but are typically converted into dry fumes values and/or reference oxygen content. These process variables are then managed by a feed-forward/feed-back control architecture, which tends to dose solid sorbent in large excess with respect to the stoichiometric to guarantee a strong neutralization and then respect limits at stack emissions. In addition, an override control logic is implemented for safety reasons: when HCl concentration measured at SMP2 overcomes a predetermined threshold, the maximum flow rate value of sorbent is promptly fed.

Therefore, identifying a suitable process model is the first step for the design of advanced model-based controllers able to improve process control and economic performance, since then sorbent levels can be optimized and solid residuals can be minimized.

2.2 Variables definition

The following two systems are investigated to describe the first stage of acid gas removal.

- Case I - 2 inputs, 1 output system:
  - inputs (u) are i) the inlet concentration of HCl expressed in [mg/Nm^3] measured at SMP1 (Figure 1); ii) the input mass flow rate of $Ca(OH)_2$ in [kg/h], evaluated from the rotational speed of the dosing screw feeder;
  - output (y) is the outlet concentration of HCl, in [mg/Nm^3], measured at SMP2.
- Case II - 3 inputs, 2 outputs system:
  - inputs: the previous i) and ii), plus iii) the pressure of compressed air injected over the first baghouse to break and remove the solid cake, expressed as a binary variable (1 - no air, 0 - air);
  - outputs: the previous i), plus ii) the pressure drop across the first baghouse, in [mbar], at SMP2.

Input-output data are collected with a sampling time $T_s = 60$ s.

3. SYSTEM IDENTIFICATION AND VALIDATION

To identify reliable dynamic models for the first removal stage by using input-output data obtained from plant tests, the open-source Systems Identification Package for PYthon (SIPPY) (Armenise et al., 2018) was adopted. Different linear model structures and orders were considered and then compared. Two datasets (A,B) were used for identification purpose, other two (C,D) were employed for model validation.

3.1 Input design

While inlet concentration of HCl is a disturbance variable, which depends on the composition of the waste fractions treated in the plant, flow rate of $Ca(OH)_2$ is a standard manipulated variable, which can be actually varied by control room operators. Therefore, the present control system was partially deactivated and two different Generalized Binary Noise (GBN) sequences were imposed as inputs to the plant to build suitable tests for the dynamic identification of the system. GBN sequences are very effective signals for identification purposes, since they show a sufficiently high power spectrum in mid and low frequency range, and then have a related appealing property, known as *persistent excitation* (Zhu, 2001). On the opposite, traditional step signals have limited frequency content and do not always excite the plant significantly.

A GBN signal has two only possible values $\{+a, -a\}$. Defined $p_{sw} \in (0,1)$ as the *switching probability*, the signal u obeys to:

$$\begin{cases} P[u_k = -u_{k-1}] & = p_{sw} \\ P[u_k = u_{k-1}] & = 1 - p_{sw} \end{cases} \quad (4)$$

where P is the probability and subscript k denotes the $k-th$ sampling time. Figure 2 shows the input data sequences obtained during the two tests on the plant. The various parameters of GBN were properly calibrated according to the indications given by Zhu (2001). In particular:

- test duration was set to 8 hours, that is, around 10 times the main process settling time ($T_{set} = 50$ min), which was known from previous data analysis and from plant operators' experience;
- minimum number of samples and corresponding minimum time period between two consecutive switches - set to limit operators' effort - were $N_{sw}^{min} = 10$ and $T_{sw}^{min} = N_{sw}^{min} \cdot T_s = 10$ min;

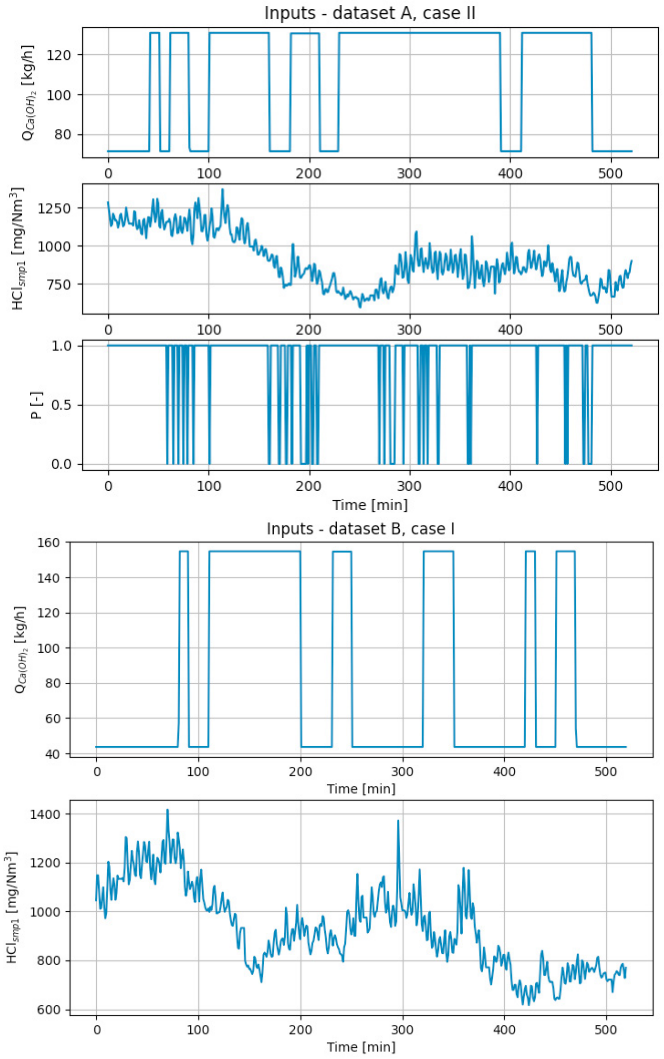

Fig. 2. Time trends of inputs for the two GBN tests: top) dataset A, Case II; bottom) dataset B, Case I.

GBN	Q_m	$\bar{Q}$	ΔQ [kg/h]	ΔU [%]	$\overline{\text{HCl}}_{in}$ [mg/Nm^3]
A)	100	111.4	$\simeq$ 70 - 130	18 - 33	905.9
B)	100	81.5	$\simeq$ 45 - 155	11 - 39	931.7

Table 1. Parameters adopted for the input GBN sequences of $Ca(OH)_2$.

- Mean Switching Time, that is, the average time period between two consecutive switches, was imposed as: $ET_{sw} = \max(40 \text{ min}; 0.98\frac{T_{set}}{3})$;
- Switching probability was thus evaluated as $p_{sw} = \frac{T_{sw}^{min}}{ET_{sw}}$.

Table 1 synthesizes the other parameters adopted for the two sequences of mass flow rate of $Ca(OH)_2$ fed to the reactor, Q_m and $\bar{Q}$ are the median and mean values, respectively; ΔQ is the amplitude (min - max) in terms of flow rate; ΔU is the variation in the corresponding screw feeder rotational speed (scaled value in % of max velocity), which is the actual manipulated variable; $\overline{\text{HCl}}_{in}$ is the average value of hydrogen chloride entering the reactor during the test. Note that amplitudes of GBNs were arranged with operators to have a compromise between significant excitation of the output and sustainable perturbation for the whole plant.

3.2 Identification

As said, the two input-output datasets obtained when applying the GBN sequences to $Ca(OH)_2$ flow rate were used for identification scope. Different model structures and various orders were tested and then compared. As input-output models, the well-known AutoRegressive and AutoRegressive–Moving-Average with eXogenous inputs models, that is, ARX and ARMAX models, were tested. A MISO approach is carried out for both systems (Case I and II); so that, for ARMAX, it holds:

$$\begin{aligned} y_k + a_1 y_{k-1} + \cdots + a_{n_a} y_{k-n_a} &= b_{1,1} u^{(1)}_{k-\theta_1-1} + \cdots \\ &+ b_{1,n_{b1}} u^{(1)}_{k-\theta_1-n_{b1}} + \cdots + b_{m,1} u^{(m)}_{k-\theta_m-1} + \cdots \\ &+ b_{m,n_{bm}} u^{(m)}_{k-\theta_m-n_{bm}} + e_k + c_1 e_{k-1} + \cdots + c_{n_c} e_{k-n_c} \end{aligned} \quad (5)$$

where n_a denotes the output order, n_{bi} the order of the *i-th* input, θ_i the delay of the *i-th* input, n_c the error model order, a_j the *j-th* coefficient of the output, $b_{i,j}$ the *j-th* coefficient of the *i-th* input and c_j denotes the *j-th* coefficient of the error model. ARX models, with no error model ($n_c = 0$), are identified with simple linear least-square (LLS) regression by computing the pseudo-inverse of the regressor matrix. ARMAX models, which instead require a pseudo-linear regression, are obtained by LLS within a suitable iterative procedure (Bacci di Capaci et al., 2021).

To identify state-space (SS) models, the *innovation form* is employed:

$$\begin{cases} x_{k+1} = Ax_k + Bu_k + Ke_k \\ y_k = Cx_k + Du_k + e_k \end{cases} \quad (6)$$

where $x_k \in \mathbb{R}^n$, $w_k \in \mathbb{R}^n$, and $v_k \in \mathbb{R}^p$ are the system state, state noise, and output measurement noise, respectively. $A \in \mathbb{R}^{n\times n}$, $B \in \mathbb{R}^{n\times m}$, $C \in \mathbb{R}^{p\times n}$, $D \in \mathbb{R}^{p\times m}$ are the system matrices, while K is the steady-state *Kalman filter gain*, obtained from Algebraic Riccati Equation. As identification method, an established subspace method with parsimonious algorithm (PARSIM-K) was adopted (Pannocchia and Calosi, 2010).

Tables 2 and 3 summarize the identification results for the various model orders in terms of fitting of the output data for Case I and Case II, respectively. In particular, as performance index, the Explained Variance, falling into $[1, -\infty)$, is reported:

$$EV = 1 - \frac{\frac{1}{N}\sum_{i=1}^{N}(\hat{y}_i - y_i)^2}{\sigma_y^2} \quad (7)$$

where $\hat{y}$ is the model output sequence, $\sigma_y^2 = \frac{1}{N}\sum_{i=1}^{N}(\bar{y} - y_i)^2$ is the variance of the actual output y, with respect to its mean value $\bar{y}$, being N the number of time samples. Note that EV is equal to the well-known coefficient of determination R^2. Input-output models show a slightly better performance than state-space formulation, as higher values of EV are obtained. In particular, ARMAX models, by describing the error dynamics with a moving average term, gives the best outcomes.

The identification results obtained on dataset B) for selected 2x1 models (Case I) - ARX[2, (2, 2), (1, 1)], ARMAX[2, (2, 2), 2, (1, 1)], and SS[7] - are further discussed. Note that the order of the SS model is here obtained with the well-known Akaike Information Criterion (AIC) by setting a threshold on the underlying singular values. Bacci di Capaci et al. (2021). Figure 3 shows the different time trends of the output HCl concentration: measured values at SMP2 are compared with the ones obtained by the three model structures. Moreover, in Figure 4 the unit step responses obtained from the two input-output identified dynamics are reported. In particular, discrete

Case I - 2x1 Models [Orders]	**Dataset**	*EV*						**Mean** *EV*
		[1,(1,1),(0,0)]	[1,(1,1),(1,1)]	[1,(1,1),(2,2)]	[2,(2,2),(0,0)]	[2,(2,2),(1,1)]	[3,(3,3),(0,0)]	
ARX $[n_a,(n_{bi}),(\theta_i)]$	A)	95.65	95.72	95.72	97.00	97.07	97.19	**96.39**
	B)	97.60	97.55	97.50	98.27	98.35	98.39	**97.61**
		[1,(1,1),1,(0,0)]	[1,(1,1),1,(1,1)]	[1,(1,1),1,(2,2)]	[2,(2,2),2,(0,0)]	[2,(2,2),2,(1,1)]	[3,(3,3),3,(0,0)]	
ARMAX $[n_a,(n_{bi}),n_c,(\theta_i)]$	A)	96.77	96.86	96.80	97.14	97.18	97.22	**96.99**
	B)	98.23	98.27	98.17	98.32	98.39	98.41	**98.30**
		[4]	[5]	[6]	[7]	[8]	AIC [1-9]	
SS $[n]$	A)	96.82	96.74	96.78	96.81	96.89	96.86 [9]	**96.82**
	B)	98.02	97.90	97.93	97.78	97.77	97.78 [7]	**97.83**

Table 2. Identification stage. Performance results for two datasets with different model orders (Case I).

Case II - 3x2 Models [Orders]	*EV*						**Mean** *EV*
ARX $[n_a,(n_{bi}),(\theta_i]$	[(1,1),(**1**),(**0**)] 96.67	[(1,1),(**1**),(**1**)] 96.70	[(1,1),(**1**),(**2**)] 96.70	[(2,2),(**2**),(**0**)] 97.72	[(2,2),(**2**),(**1**)] 97.77	[(3,3),(**3**),(**0**)] 97.89	**97.24**
ARMAX $[n_a,(n_{bi}),n_c,(\theta_i)]$	[(1,1),(**1**),(1,1),(**0**)] 97.52	[(1,1),(**1**),(1,1),(**1**)] 97.60	[(1,1),(**1**),(1,1),(**2**)] 97.55	[(2,2),(**2**),(2,2),(**0**)] 97.83	[(2,2),(**2**),(2,2),(**1**)] 97.87	[(3,3),(**3**),(3,3)(**0**)] 97.92	**97.71**
SS $[n]$	[5] 57.20	[6] 68.77	[7] 71.32	[8] 71.84	[9] 58.73	AIC [1-9] 29.43 [4]	**59.54**

Table 3. Identification stage. Performance results for dataset A with different model orders (Case II).

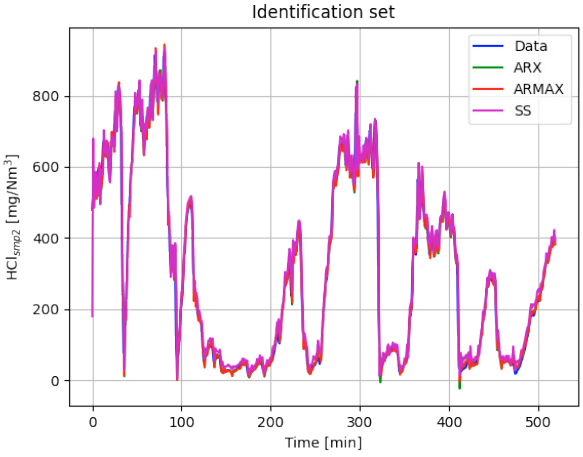

Fig. 3. Output time trends: real data and selected model responses (Case I, dataset B).

time transfer functions $G_{1i}(z) = \frac{B_{1i}(z)}{A_1(z)}$, being $A_1(z)$ and $B_{1i}(z)$ the corresponding polynomials in z operator for the dynamics between *i-th* input and the single output 1, are investigated. As a matter of fact, similar behaviors are obtained for ARX and ARMAX models, since values of the static gain ($K_{11} \simeq -3.05$; $K_{12} \simeq 0.63$) and settling times ($T_{11,set} \simeq 30$ min; $T_{12,set} \simeq 35$ min) are pretty close. It also worth noting that expected steady-state results are obtained: single increases of $Ca(OH)_2$ dosage and of inlet HCl concentration cause a decrease and an increase of outlet HCl concentration, respectively; that is, $K_{11} < 0$ and $K_{12} > 0$.

Finally, the identification results obtained on dataset A) for two selected 3x2 models (Case II) are illustrated: we consider ARX$[(2,2),([\mathbf{2}]),([\mathbf{1}])]$ and ARMAX$[(2,2),([\mathbf{2}]),(2,2),([\mathbf{1}])]$. Note that we did not report results for any SS models since their performance are lower in this scenario. Figure 5 shows the time trends of output HCl concentration and of pressure drop across the first baghouse ΔP: measured values are compared with the ones obtained by the two input-output models. In Figure 6, the unit step responses obtained from the two identified dynamics are reported. One can observe that once a shot of compressed

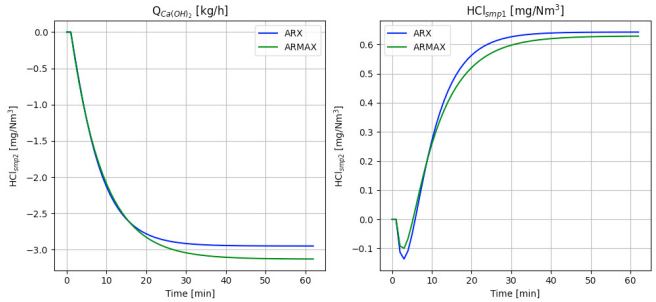

Fig. 4. Step tests for two selected ARX and ARMAX dynamics (Case I, dataset B).

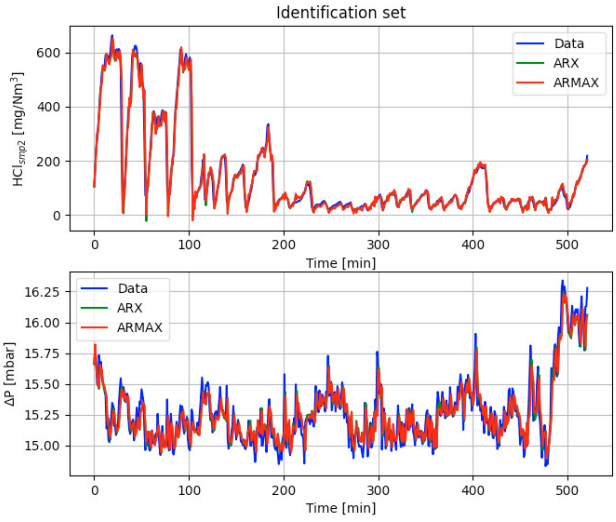

Fig. 5. Output time trends: real data and selected model responses (Case II, dataset A).

air is injected, i.e., when a positive variation of pressure P is applied: i) an evident inverse response for the outlet HCl concentration is obtained, i.e., after a transient increase due to remixing effects, the steady-state effect is beneficial since final value is significantly smaller ($K_{13} < 0$); ii) the pressure drop across the first baghouse monotonically decreases ($K_{23} < 0$), meaning that the solid cake of chemical residuals is actually broken and then removed.

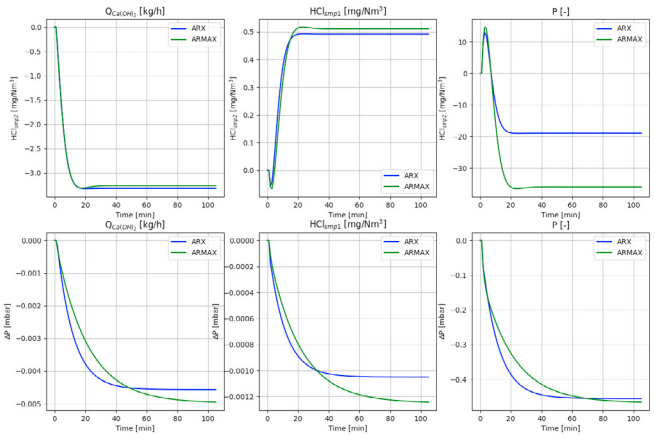

Fig. 6. Step tests for two selected ARX and ARMAX dynamics (Case II, dataset A).

3.3 Validation

Two different routine datasets were used for model validation, once the original industrial control system was restored. Figure 7 shows the input data sequences: $Ca(OH)_2$ flow rate reveals several sharp peaks towards its maximum feed rate value; this means that the control override logic gets activated as output HCl concentration overcomes the predetermined safety threshold ($\simeq$600 mg/Nm^3), and this occurs several times (compare Figure 8). This fact makes the validation datasets very different from the GBN sequences and then generates a particularly challenging scenario for the identified models.

The different model structures previously identified were tested and then compared. Table 4 and 5 summarize the validation results for the various model orders, for Case I and II, respectively; output data fitting is again evaluated by computing the index EV. Note that these results are for standard validation, that is, when input-output data are used to predict the model response one-step ahead in the future. For example, for ARX and ARMAX the following predictor is adopted (Ljung, 1999):

$$\hat{y}_{k|k-1} = H^{-1}(z)G(z)u_k + (1 - H^{-1}(z))y_k \tag{8}$$

where $G(z)$ and $H(z)$ are the identified transfer matrices relating the output with deterministic input u and stochastic noise e, respectively. For SS model, the innovation form is again considered to exploit the identified K matrix. Input-output models confirm slightly better performance than the state-space formulation, as higher values of EV are obtained, especially for Case II. Again, ARMAX models, due to its error model term, gives the best outcomes. The results obtained on dataset C) for selected 3x2 models (Case II) are further illustrated: ARX$[(2,2),(\mathbf{2}),(\mathbf{1})]$, ARMAX$[(2,2),(\mathbf{2}),(2,2),(\mathbf{1})]$. Figure 8 shows the different time trends of measured values (output HCl concentration and pressure drops ΔP) compared with the ones from the two input-output models.

In addition, for the two input-output models a general r-step ahead validation is performed, where the following predictor is computed (Zhao et al., 2014):

$$\hat{y}_{k|k-r} = W_r(z)G(z)u_k + (1 - W_r(z))y_k \tag{9}$$

where $W_r(z) = \bar{H}_r(z)H^{-1}(z)$, being $\bar{H}_r(z) = \sum_{j=0}^{r-1} h_j z^{-j}$ a suitable discrete time transfer function, where $\{h_j\}$ are the coefficients of the finite impulse response of $H(z)$. Table 6 shows the validation results for different values of the horizon r applied to the 2x1 system (Case I). Awaited results are obtained: larger horizons imply lower prediction performance, and ARMAX models outperforms ARX. Nevertheless, both input-output models can be considered sufficiently reliable for control purpose and can be implemented into advanced control structures to improve the process operation.

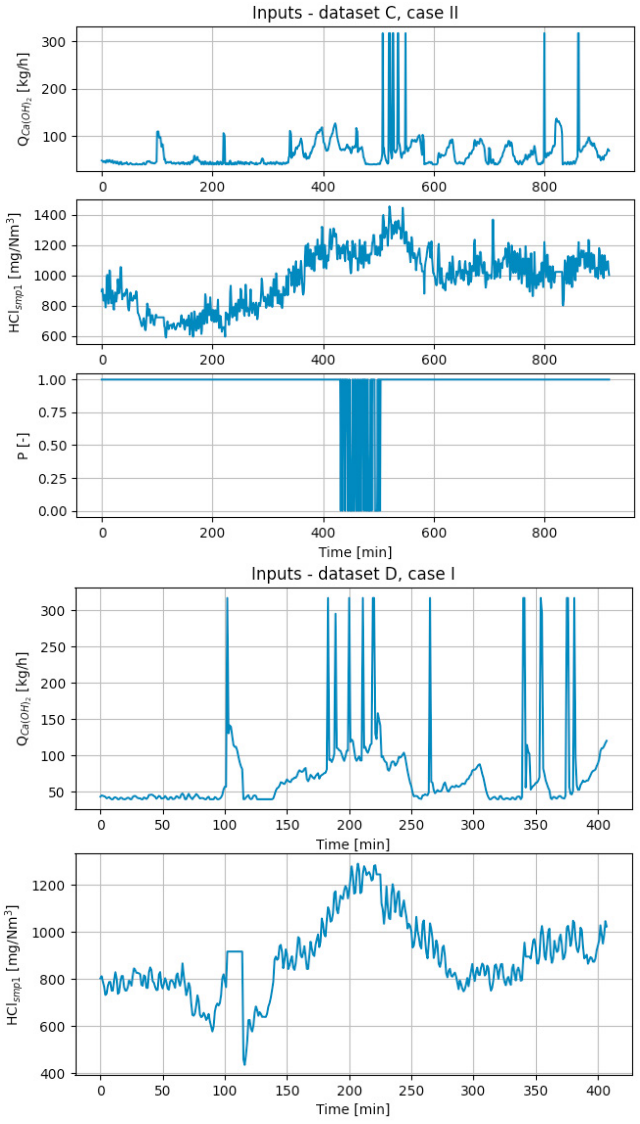

Fig. 7. Time trends of input data used for validation purpose: top) dataset C, Case II; bottom) dataset D, Case I.

4. CONCLUSIONS

Regulation of acid gas treatment units within waste-to-energy plants represents a relevant and challenging control problem, as the amplitude and volatility of process disturbances destabilize traditional control schemes. In this paper, different data-driven models were tested and compared as a first and necessary step in the design of advanced control systems for WtE acid gas removal. A two-stage acid gas treatment line of an Italian plant was taken as case study. GBN tests of varying reactant flow rate were carried out to produce datasets for system identification. Different input-output and state-space models were identified, optimized and then cross-validated on data of normal plant operation. ARMAX, ARX, and also SS models offered acceptable results in terms of prediction, with a slightly higher performance for the former. Having proved the suitability of the proposed models, future work will be focused on their

Case I - 2x1 Models [Orders]	**Dataset**	*EV*						**Mean** *EV*
		[1,(1,1),(0,0)]	[1,(1,1),(1,1)]	[1,(1,1),(2,2)]	[2,(2,2),(0,0)]	[2,(2,2),(1,1)]	[3,(3,3),(0,0)]	
ARX $[n_a,(n_{bi}),(\theta_i)]$	C)	89.62	89.81	89.56	90.02	90.35	89.83	**89.86**
	D)	82.57	82.65	82.70	83.07	83.38	83.51	**82.98**
		[1,(1,1),1,(0,0)]	[1,(1,1),1,(1,1)]	[1,(1,1),1,(2,2)]	[2,(2,2),2,(0,0)]	[2,(2,2),2,(1,1)]	[3,(3,3),3,(0,0)]	
ARMAX $[n_a,(n_{bi}),n_c,(\theta_i)]$	C)	90.05	90.58	91.07	90.28	91.06	90.39	**90.57**
	D)	83.62	83.64	84.90	85.17	86.36	86.57	**85.04**
		[4]	[5]	[6]	[7]	[8]	AIC [1-9]	
SS $[n]$	C)	90.03	90.49	89.53	89.63	89.90	89.48 [9]	**89.84**
	D)	83.13	83.67	84.25	84.41	83.41	84.41 [7]	**82.92**

Table 4. Validation stage. Performance results for two datasets for different model orders (Case I).

Case II - 3x2 Models [Orders]	*EV*						**Mean** *EV*
ARX $[n_a,(n_{bi}),(\theta_i]$	[(1,1),(**1**),(**0**)] 96.07	[(1,1),(**1**),(**1**)] 96.15	[(1,1),(**1**),(**2**)] 96.28	[(2,2),(**2**),(**0**)] 96.54	[(2,2),(**2**),(**1**)] 96.73	[(3,3),(**3**),(**0**)] 96.85	**96.43**
ARMAX $[n_a,(n_{bi}),n_c,(\theta_i)]$	[(1,1),(**1**),(1,1),(**0**)] 97.09	[(1,1),(**1**),(1,1),(**1**)] 97.23	[(1,1),(**1**),(1,1),(**2**)] 97.39	[(2,2),(**2**),(2,2),(**0**)] 97.21	[(2,2),(**2**),(2,2),(**1**)] 97.37	[(3,3),(**3**),(3,3)(**0**)] 97.21	**97.25**
SS $[n]$	[5] 78.94	[6] 83.59	[7] 85.97	[8] 85.91	[9] 79.46	AIC [1-9] 66.9 [4]	**80.13**

Table 5. Validation stage. Performance results for dataset C with different model orders (Case II).

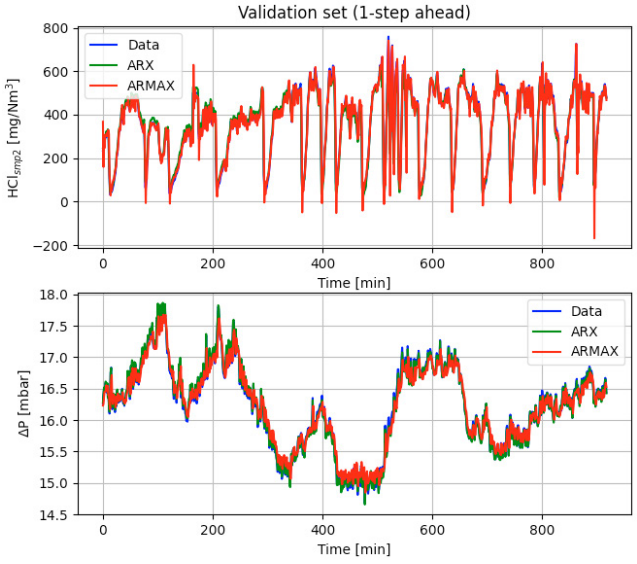

Fig. 8. Output time trends in validation: real data and selected model responses (Case II, dataset C).

Model [Orders]	**Dataset**	*EV*					
ARX		$r=2$	3	4	5	7	10
$[2,(2,2),(1,1)]$	C)	70.51	57.83	48.03	40.81	27.95	21.25
	D)	59.24	33.45	22.88	17.63	3.81	2.75
ARMAX		$r=2$	3	4	5	7	10
$[2,(2,2),2,(1,1)]$	C)	76.22	60.94	50.59	42.54	30.06	23.14
	D)	61.54	36.14	25.28	19.08	5.98	4.63

Table 6. r-step ahead validation: performance results for different prediction horizons (Case I).

integration in advanced control structures. In particular, model-based architectures (IMC and MPC) will be derived and tested on simulation and industrial data, and then compared with the current suboptimal control logic in order to increase the process performance.

REFERENCES

Armenise, G., Vaccari, M., Bacci di Capaci, R., and Pannocchia, G. (2018). An open-source system identification package for multivariable processes. In *2018 UKACC 12th International Conference on Control (CONTROL)*, 152–157. IEEE.

Bacci di Capaci, R., Vaccari, M., Armenise, G., and Pannocchia, G. (2021). Systems Identification Package for Python (SIPPY): User Guide. https://github.com/CPCLAB-UNIPI/SIPPY.

Biganzoli, L., Racanella, G., Rigamonti, L., and Grosso, M. (2015). High temperature abatement of acid gases from waste incineration. Part ii: Comparative life cycle assessment study. *Waste Management*, 35, 127–134.

Dal Pozzo, A., Antonioni, G., Guglielmi, D., Stramigioli, C., and Cozzani, V. (2016). Comparison of alternative flue gas dry treatment technologies in waste-to-energy processes. *Waste Management*, 51, 81–90.

Dal Pozzo, A., Guglielmi, D., Antonioni, G., and Tugnoli, A. (2017). Sustainability analysis of dry treatment technologies for acid gas removal in waste-to-energy plants. *Journal of Cleaner Production*, 162, 1061–1074.

Dal Pozzo, A., Guglielmi, D., Antonioni, G., and Tugnoli, A. (2018a). Environmental and economic performance assessment of alternative acid gas removal technologies for waste-to-energy plants. *Sustainable Production and Consumption*, 16, 202–215.

Dal Pozzo, A., Moricone, R., Antonioni, G., Tugnoli, A., and Cozzani, V. (2018b). Hydrogen chloride removal from flue gas by low-temperature reaction with calcium hydroxide. *Energy and Fuels*, 32(1), 747–756.

Dal Pozzo, A., Muratori, G., Antonioni, G., and Cozzani, V. (2021). Economic and environmental benefits by improved process control strategies in HCl removal from waste-to-energy flue gas. *Waste Management*, 125, 303–315.

Ljung, L. (1999). *System Identification: Theory for the User*. Prentice Hall Inc., Upper Saddle River, New Jersey, second edition.

Pannocchia, G. and Calosi, M. (2010). A predictor form PARSIMonious algorithm for closed-loop subspace identification. *Journal of Process Control*, 20(4), 517–524.

Zhao, J., Zhu, Y., and Patwardhan, R. (2014). Identification of k-step-ahead prediction error model and MPC control. *Journal of Process Control*, 24(1), 48–56.

Zhu, Y. (2001). *Multivariable System Identification For Process Control*. Elsevier Science, first edition.